LASER & PHOTONICS REVIEWS

www.lpr-journal.org

Fundamental Distinction of Electromagnetically Induced Transparency and Autler–Townes Splitting in Breaking the Time-Reversal Symmetry

Haodong Wu, Yaping Ruan, Zhixiang Li, Ming-Xin Dong, Miao Cai, Jiangshan Tang, Lei Tang, Han Zhang, Min Xiao,* and Keyu Xia**

Despite the essential difference in underlying physics, electromagnetically induced transparency (EIT) and Autler–Townes splitting (ATS) are difficult to be discriminated because they cause resemble absorption and dispersion to a probe electromagnetic field. They are mainly discerned in the sense of absorption profile fitting. Here, the breakdown of the time-reversal symmetry (TRS), namely optical nonreciprocity in the EIT and ATS configurations are experimentally observed by using warm rubidium atoms. The microscopic Doppler effect due to atomic thermal motion causes strong optical nonreciprocity to the probe field in the EIT configuration. In stark contrast, the propagation of the probe field is primarily reciprocal in the ATS configuration. The experimental observations in this study objectively distinguish the EIT and ATS effects in the fundamental physics of breaking the TRS. This experiment proves a concept of using the TRS as a testbed for discerning fundamental physical effects.

1. Introduction

Electromagnetically induced transparency (EIT)[1] and Autler–Townes splitting (ATS)[2,3] are two fundamental effects in quantum optics and play important roles in quantum science and technology. The ATS is also referred to as the dynamic Stark shift. Both the effects can cause an absorptive medium transparent but are fundamentally distinct in underlying physics. It is of great interest to deeply understand what is the distinction in underlying physics behind EIT and ATS.

EIT originates from the destructive interference of two quantum pathways.[1,4,5] It is typically realized in Λ-type or ladder-type quantum systems. The EIT concept is now extended to optomechanical systems,[6,7] acoustic systems,[8] solid-state photonic circuits,[9–11] superconducting circuits,[12] plasmonic systems,[13] and even cavity quantum electrodynamics systems.[14–16] EIT has been widely used for cooling of mechanical motion,[17] quantum memory of photons,[18] slow light,[10,19,20] and enhancement of optical nonlinearity.[21–30] Recently, experimental observations and theoretical studies find that thermal-motion-induced chiral EIT in warm atoms can lead to optical nonreciprocity due to the susceptibility-momentum locking (SML).[31–35]

Unlike EIT, ATS is rooted in energy level splitting due to the strong control field and has been widely observed in various systems such as color defects in nanodiamond,[36] 2D materials, and transition metal dichalcogenides.[37–39] It also demonstrates an important manner for quantum manipulation such as optical switching,[40] photon storage,[41] single-photon isolation.[42]

Although both EIT and ATS effects are intensively studied, identifying them in a practical case is still challenging because of their similarity phenomena in experimental observation.[43–45] This similarity has caused a debate about the existence of EIT in a V-type system.[1,43,44,46] Revealing the distinct physics involved in EIT and ATS are crucial for fundamental physics and applications. Their difference is discussed by comparing the transparent window width.[5,47,48] By numerically fitting the experimentally observed absorption profile, one can calculate the Akaike information criterion (AIC) weights of EIT and ATS contributions and then use the weights to distinguish them.[49–53] The AIC weights

H. Wu, Y. Ruan, Z. Li, M. Cai, L. Tang, K. Xia
College of Engineering and Applied Sciences, and National Laboratory of Solid State Microstructures
Nanjing University
Nanjing 210023, China
E-mail: keyu.xia@nju.edu.cn

M.-X. Dong
Key Laboratory of Quantum Information
University of Science and Technology of China
Hefei, Anhui 230026, China

J. Tang, H. Zhang
School of Physics
Nanjing University
Nanjing 210023, China
E-mail: zhanghan@nju.edu.cn

M. Xiao
Department of Physics
University of Arkansas
Fayetteville, AR 72701, USA
E-mail: mxiao@uark.edu

K. Xia
Jiangsu Key Laboratory of Artificial Functional Materials
Nanjing University
Nanjing 210093, China

The ORCID identification number(s) for the author(s) of this article can be found under https://doi.org/10.1002/lpor.202100708

DOI: 10.1002/lpor.202100708

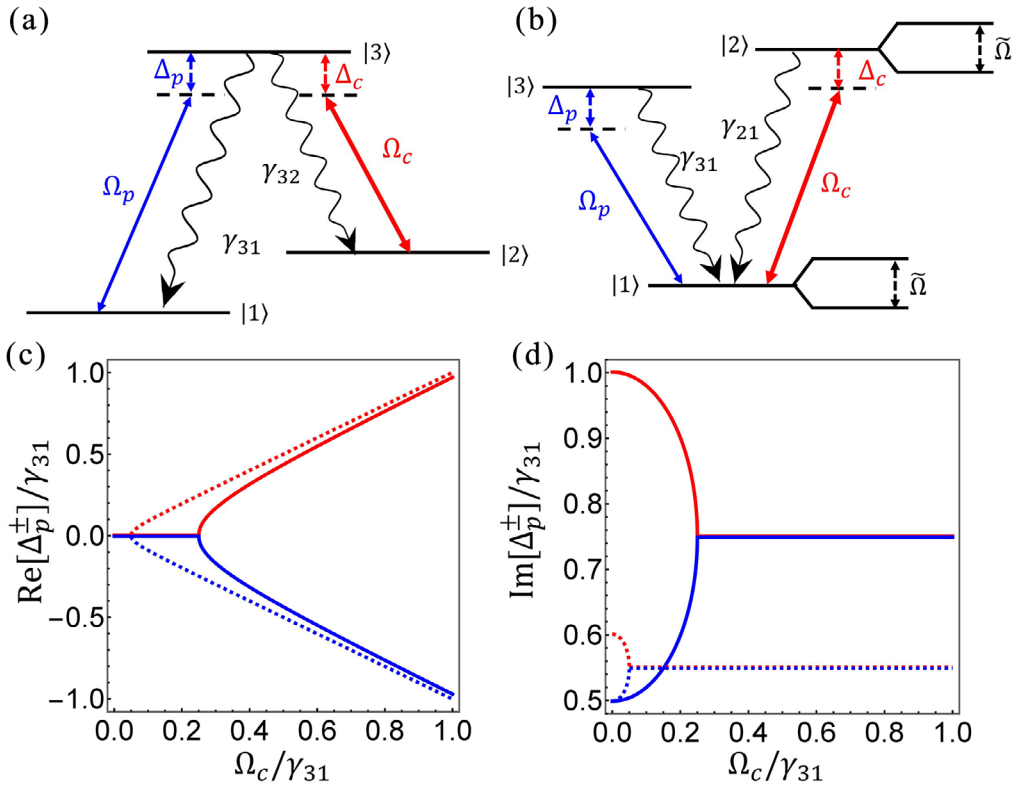

Figure 1. a) EIT configuration using a Λ-type system with two ground states $|1\rangle$ and $|2\rangle$, and one common excited state $|3\rangle$. b) ATS configuration using a *V*-type system with two excited states $|3\rangle$ and $|2\rangle$, and one common ground state $|1\rangle$. The strong control field Ω_c drives the transition between states $|2\rangle$ and $|3\rangle$ with a detuning Δ_c. The probe field Ω_p couples to the transition of $|1\rangle \leftrightarrow |3\rangle$ with a detuning $\Delta_p^{\pm}$. The control field in (b) causes the ATS $\widetilde{\Omega}$. c,d) Represent the real and imaginary parts of $\Delta_p^{\pm}$, respectively. Red and blue curves are the positive and negative frequency modes, respectively. Two modes merge into one at exception point $\Omega_c^{EP} = 0.45\gamma_3$ when $\Gamma_{21} = 0.1\gamma_3$ and $\Omega_c^{EP} = 0.05\gamma_3$ when $\Gamma_{21} = 1.2\gamma_3$.

gradually vary with the coupling strength indicates a smooth transition from EIT to ATS.

A natural question arises: Whether EIT and ATS can lead to any distinct experimental observation implying fundamentally different physics? The answer to this question will deepen our understanding of these two physical effects.

In this paper, we report an experiment measuring optical nonreciprocity to objectively discriminate the EIT and ATS effects in warm rubidium (Rb) atoms. Because of the thermal-motion induced SML in the EIT configuration, the TRS of a probe light breaks, leading to nonreciprocal transmission. In stark contrast, the atomic medium in the ATS configuration causes little nonreciprocity to the probe propagation. This different capability in breaking the TRS provides a new view angle to interpretation of the EIT and ATS effects.

2. Theoretical Analysis

This work aims to provide a discrimination of EIT and ATS with optical nonreciprocity in the Λ-type system for the EIT configuration and in the V-type system for the ATS configurations, see **Figure 1**a,b. To evaluate the optical nonreciprocity in these two systems, we need to calculate the susceptibility and the resulting transmission for the probe field co- and counter-propagating with the control laser beam in both the EIT and ATS configurations. In the co-propagation case, the control and probe laser beams propagate through the atomic vapor cell from left to right. In the counter-propagation case, the control field travels from right to left, in opposite direction of the probe field.

Generally, for a *L*-long medium with susceptibility χ, the transmission of a probe field with frequency ω_p is given by

$$\mathcal{T} = \exp[-\omega_p \mathrm{Im}(\chi) L/c] \tag{1}$$

with the vacuum permittivity ϵ_0, and $\mathrm{Im}(\chi)$ being the imaginary part of χ. In our experiment, this susceptibility is determined by the relevant atomic polarization $\langle\sigma_{13}\rangle$.

We first consider the Λ-type EIT configuration with two ground states $|1\rangle$ and $|2\rangle$, and one excited state $|3\rangle$, see Figure 1a. The state $|3\rangle$ decays to states $|1\rangle$ and $|2\rangle$ with rates γ_{31} and γ_{32}, respectively. We denote γ_3 as the total decoherence rate of state $|3\rangle$. In the standard theoretical model, $\gamma_3 = \gamma_{31} + \gamma_{32}$ when the dephasing and linewidth broadening are excluded. The dephasing rate between two ground states is denoted as Γ_{21}. The control field Ω_c (probe field Ω_p) drives the atomic transition between $|2\rangle$ and $|3\rangle$ ($|1\rangle$ and $|3\rangle$) with a detuning Δ_c (Δ_p). In a properly rotating frame, the Hamiltonian describing the dynamics of this EIT configuration takes the form in the absence of the Doppler effect

$$H_{\mathrm{EIT}} = -\Delta_p\sigma_{11} - \Delta_c\sigma_{22} + \Omega_p(\sigma_{13} + \sigma_{31}) + \Omega_c(\sigma_{23} + \sigma_{32}) \tag{2}$$

where Pauli operators σ_{ij} are defined as $\sigma_{ij} = |i\rangle\langle j|$ with $i,j \in \{1,2,3\}$, the field-atom detunings are $\Delta_p = \omega_3 - \omega_1 - \omega_p$ and $\Delta_c = \omega_3 - \omega_2 - \omega_c$ for the control and probe lasers, respectively.

We are interested in the steady-state transmission spectrum. In our experiment, hot atoms at temperature T move randomly with a Maxwell–Boltzmann velocity distribution of $D(v) = e^{-v^2/v_p^2}/\sqrt{\pi}v_p$, where v is the velocity of atoms, the mean velocity is $v_p = \sqrt{2k_B T/m}$ and m is the atomic mass and k_B for the Boltzmann constant. This thermal motion causes microscopic Doppler shifts in atom-light interaction. To a good approximation, we assume that the control and probe fields have the same wave number k. Here, we only need to consider the longitudinal Doppler shift but can neglect the transverse contribution.[31] For the control field approaching to an atom with velocity v, the longitudinal Doppler shift is kv. When the probe field co-propagates with the control field in this EIT configuration, atoms "see" the same Doppler shifts. The corresponding susceptibility is given by[31]

$$\chi_{EIT}^{f}(v) = \int_{-\infty}^{+\infty} \frac{-iD(v)N\mu_{13}^2/\varepsilon_0}{i(\Delta_p + kv) + \frac{\gamma_3}{2} + \frac{\Omega_c^2}{i(\Delta_p - \Delta_c) + \frac{\Gamma_{21}}{2}}} dv \quad (3)$$

where N is the atomic number density populated in state $|1\rangle$, and $\mu 13$ is the dipole moment of the transition $|1\rangle \leftrightarrow |3\rangle$. It can be seen from Equation (3) that the Doppler effect is greatly suppressed. The atomic cloud is primarily transparent to the probe field. In the counter-propagation case, atoms are always subject to opposite Doppler shifts, leading to a strong absorption. The corresponding atomic susceptibility is[31]

$$\chi_{EIT}^{b}(v) = \int_{-\infty}^{+\infty} \frac{-iD(v)N\mu_{13}^2/\varepsilon_0}{i(\Delta_p - kv) + \frac{\gamma_3}{2} + \frac{\Omega_c^2}{i(\Delta_p - \Delta_c - 2kv) + \frac{\Gamma_{21}}{2}}} dv \quad (4)$$

From Equations (3) and (4), we can see the atomic susceptibility is different by $2kv$ in the interference term and thus is locked to the propagation direction of the probe field, that is, the probe momentum, with respect to the control field. This SML can cause a directional dark-state condition and break the TRS for the probe field. We obtain the transmission by replacing χ in Equation (1) with χ_{EIT}^{f} or χ_{EIT}^{b}. Thus, the probe transmission in this EIT configuration shows strong optical nonreciprocity because of the SML.[31,33–35]

According to our understanding, the transition from EIT to ATS profile in the AIC-based fitting is actually the transition of the EIT profile at exceptional point. For simplicity, we consider the case without the Doppler effect in Equations (3) and (4), which is the case for the AIC method.[49–53] The EIT configuration can be considered as a system with two coupled two-level systems or cavity modes. The complex eigenvalues of system are given by $\Delta_p^{\pm} = \frac{\Delta_c}{2} + i\frac{\Gamma_{21}+\gamma_3}{4} \pm \sqrt{\Omega_c^2 + \frac{1}{4}[\Delta_c + i\frac{\gamma_3 - \Gamma_{21}}{2}]^2}$. When $\Delta_c = 0$, these two eigenvalues show bifurcation at exception point (EP) $\Omega_c^{EP} = |\gamma_3 - \Gamma_{21}|/4$, see Figure 1c,d. Due to a finite temperature, the dephasing of the ground state can be large. For $\Gamma_{21} = 1.2\gamma_3$ used in the transmission fitting afterward, Ω_c^{EP} is very small, about $0.05\gamma_3$. This critical control coupling Ω_c^{EP} is exactly used as the critical value for discerning EIT and ATS in a Λ-type system with the AIC method. This EP is blur and may deviate from this estimation in experiment because of the ensemble average over the velocity. When $\Omega_c < \Omega_c^{EP}$, $\Delta_{p\pm}$ have different imaginary parts but the same real part. The absorption profile is the result of interference of two absorptive channels with different dissipative rates. In comparison, when $\Omega_c > \Omega_c^{EP}$, the imaginary parts of $\Delta_{p\pm}$ become degenerate but their real parts are different. In this case, the coupling system becomes two subsystems with different resonance frequencies. As a result, the interference of the absorptive channels gradually disappears due to the increasing detuning of these two subsystems. Therefore, the profile transition in the AIC method can be understood as the absorption change of a two coupled system crossing exceptional point. Nevertheless, the nonreciprocity underlying the EIT cannot be revealed in the AIC-based explanation.

The V-type system is very suitable for studying the ATS because the EIT effect is absent. Next we consider a V-type system shown in Figure 1b. The three-level system consists of one ground states $|1\rangle$, and two excited states $|2\rangle$and $|3\rangle$. The states $|3\rangle$ and $|2\rangle$ decay to the state $|1\rangle$ with rates γ_{31} and γ_{21}, respectively. In this V-type system, the γ_{31} is the total decoherence rate of state $|3\rangle$ so that $\gamma_3 = \gamma_{31}$. The control (probe) field drives the transition $|1\rangle \leftrightarrow |2\rangle$ ($|1\rangle \leftrightarrow |3\rangle$) with an angular frequency ω_c (ω_p) and a Rabi frequency Ω_c (Ω_p).

The Hamiltonian of the V-type system in a rotating frame is

$$H_{ATS} = \Delta_p\sigma_{33} + \Delta_c\sigma_{22} + \Omega_p(\sigma_{31} + \sigma_{13}) + \Omega_c(\sigma_{12} + \sigma_{21}) \quad (5)$$

where $\Delta_p = \omega_3 - \omega_1 - \omega_p$, $\Delta_c = \omega_2 - \omega_1 - \omega_c$ and $\sigma_{ij} = |i\rangle\langle j|$ with $i,j \in \{1,2,3\}$. Here we use the same notations as the EIT configuration for simplicity.

We can roughly estimate the susceptibility of the V-type system for the probe field by using a two-level model with transition $|1\rangle \leftrightarrow |3\rangle$ and the ATS of the state $|1\rangle$. In this treatment, we neglect the small coherence contribution σ_{23}. Without the ATS, the relevant atomic polarization is $\langle\sigma_{13}\rangle = -i\Omega_p/(i\Delta_p + \frac{\gamma_{31}}{2})$. The strong control laser beam driving the transition between $|2\rangle$ and $|1\rangle$ causes the ground state $|1\rangle$ to split into two levels separate by $\widetilde{\Omega} = \sqrt{\Omega_c^2 + (\frac{\Delta_c}{2})^2}$.[2,3] The control field modifies the atomic polarization $\langle\sigma_{13}\rangle$ and subsequently the susceptibility. Without the microscopic Doppler effect, the atomic polarization is given by

$$\langle\sigma_{13}\rangle = \frac{-i\sqrt{\frac{\widetilde{\Omega} + \frac{\Delta_c}{2}}{2\widetilde{\Omega}}}}{i(\Delta_p + \widetilde{\Omega}) + \frac{\gamma_{31}}{2}} + \frac{-i\sqrt{\frac{\widetilde{\Omega} - \frac{\Delta_c}{2}}{2\widetilde{\Omega}}}}{i(\Delta_p - \widetilde{\Omega}) + \frac{\gamma_{31}}{2}} \quad (6)$$

The weights $\sqrt{(\widetilde{\Omega} + \frac{\Delta_c}{2})/2\widetilde{\Omega}}$ and $\sqrt{(\widetilde{\Omega} + \frac{\Delta_c}{2})/2\widetilde{\Omega}}$, respectively associated with the states $|2\rangle$ and $|1\rangle$ are due to the different atomic population caused by the control field. When including the microscopic Doppler effect, the ATS becomes $\widetilde{\Omega}^f = \sqrt{\Omega_c^2 + (\frac{\Delta_c + kv}{2})^2}$ and $\widetilde{\Omega}^b = \sqrt{\Omega_c^2 + (\frac{\Delta_c - kv}{2})^2}$. To conveniently compare the susceptibility in two cases, we consider the propagation direction of the probe field as the reference such that its Doppler

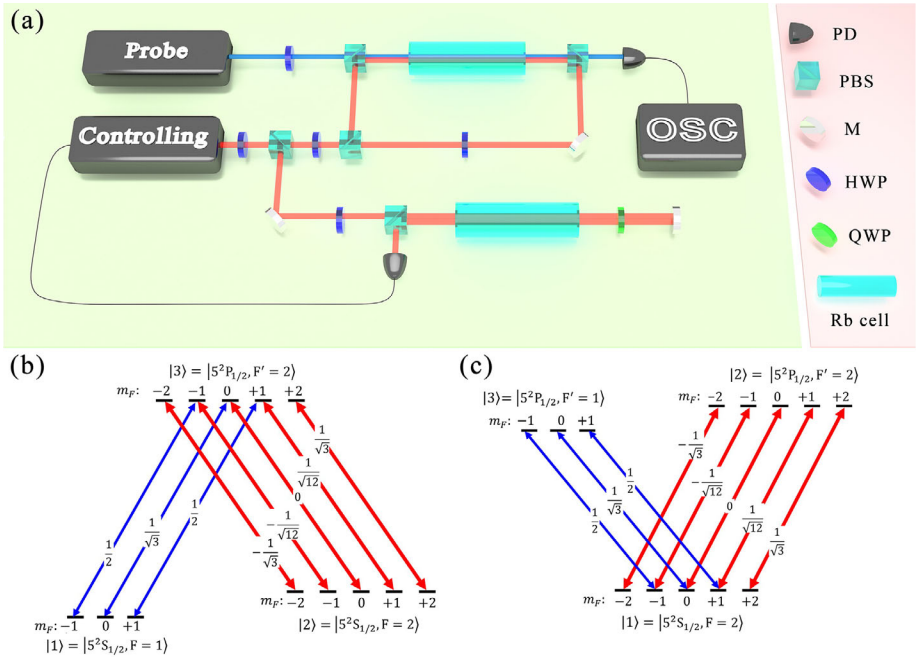

Figure 2. a) Schematic setup for observing EIT and ATS effects. PD, photon detector; PBS, polarization beam splitter; M, mirror; HWP, half-wave plate; QWP, quarter-wave plate. b) Level diagram of the EIT configuration using a ^{87}Rb atom. Two ground states are $|1\rangle = |5^2S_{1/2}, F = 1\rangle$ and $|2\rangle = |5^2S_{1/2}, F = 2\rangle$. One common excited state is $|3\rangle = |5^2P_{1/2}, F' = 2\rangle$. b) Level diagram of the ATS configuration using a ^{87}Rb atom. Two excited states are $|3\rangle = |5^2P_{1/2}, F' = 1\rangle$ and $|2\rangle = |5^2P_{1/2}, F' = 2\rangle$, and one common ground state is $|1\rangle = |5^2S_{1/2}, F = 2\rangle$. The relevant Zeeman levels and the relative strengths of the dipole transitions are also included for details.

shift is kv. Then the atomic polarization in the co- and counter-propagation cases takes the forms

$$\langle\sigma_{13}^{f}\rangle(v) = \frac{-i\sqrt{\frac{\widetilde{\Omega}^{f}+\frac{\Delta_c+kv}{2}}{2\widetilde{\Omega}^{f}}}}{i(\Delta_p+kv+\widetilde{\Omega}^{f})+\frac{\gamma_{31}}{2}} + \frac{-i\sqrt{\frac{\widetilde{\Omega}^{f}-\frac{\Delta_c+kv}{2}}{2\widetilde{\Omega}^{f}}}}{i(\Delta_p+kv-\widetilde{\Omega}^{f})+\frac{\gamma_{31}}{2}} \tag{7}$$

$$\langle\sigma_{13}^{b}\rangle(v) = \frac{-i\sqrt{\frac{\widetilde{\Omega}^{b}+\frac{\Delta_c-kv}{2}}{2\widetilde{\Omega}^{b}}}}{i(\Delta_p+kv+\widetilde{\Omega}^{b})+\frac{\gamma_{31}}{2}} + \frac{-i\sqrt{\frac{\widetilde{\Omega}^{b}-\frac{\Delta_c-kv}{2}}{2\widetilde{\Omega}^{b}}}}{i(\Delta_p+kv-\widetilde{\Omega}^{b})+\frac{\gamma_{31}}{2}} \tag{8}$$

Integrating $\langle\sigma_{13}^{b}\rangle(v)$ and $\langle\sigma_{13}^{b}(v)\rangle$ over atomic velocity gives the corresponding susceptibilities of the atomic ensemble

$$\chi_{\mathrm{ATS}}^{f} = -\int_{-\infty}^{+\infty} \frac{i\frac{N\mu_{13}^2}{\varepsilon_0}\sqrt{\frac{\widetilde{\Omega}^{f}+\frac{\Delta_c+kv}{2}}{2\widetilde{\Omega}^{f}}}}{i(\Delta_p+kv+\widetilde{\Omega}^{f})+\frac{\gamma_{31}}{2}} D(v)\,\mathrm{d}v - \int_{-\infty}^{+\infty} \frac{i\frac{N\mu_{13}^2}{\varepsilon_0}\sqrt{\frac{\widetilde{\Omega}^{f}-\frac{\Delta_c+kv}{2}}{2\widetilde{\Omega}^{f}}}}{i(\Delta_p+kv-\widetilde{\Omega}^{f})+\frac{\gamma_{31}}{2}} D(v)\,\mathrm{d}v \tag{9}$$

$$\chi_{\mathrm{ATS}}^{b} = -\int_{-\infty}^{+\infty} \frac{i\frac{N\mu_{13}^2}{\varepsilon_0}\sqrt{\frac{\widetilde{\Omega}^{b}+\frac{\Delta_c-kv}{2}}{2\widetilde{\Omega}^{b}}}}{i(\Delta_p+kv+\widetilde{\Omega}^{b})+\frac{\gamma_{31}}{2}} D(v)\,\mathrm{d}v - \int_{-\infty}^{+\infty} \frac{i\frac{N\mu_{13}^2}{\varepsilon_0}\sqrt{\frac{\widetilde{\Omega}^{b}-\frac{\Delta_c-kv}{2}}{2\widetilde{\Omega}^{b}}}}{i(\Delta_p+kv-\widetilde{\Omega}^{b})+\frac{\gamma_{31}}{2}} D(v)\,\mathrm{d}v \tag{10}$$

The susceptibilities given by Equations (9) and (10) are mainly different in the weights $\sqrt{(\widetilde{\Omega}^{f}\pm\frac{\Delta_c+kv}{2})/\widetilde{\Omega}^{f}}$ and $\sqrt{(\widetilde{\Omega}^{b}\pm\frac{\Delta_c-kv}{2})/\widetilde{\Omega}^{b}}$ of the two contributions. At $\Delta_c = 0$, we have $\widetilde{\Omega}^{f} = \widetilde{\Omega}^{b} = \sqrt{\Omega_c^2+(\frac{kv}{2})^2}$. When $\Omega_c > kv$, the influence of these terms tends to very small. By substituting χ_{ATS}^{f} or χ_{ATS}^{b} to χ in Equation (1), we obtain the transmission.

3. Experimental Section

The experiments for observing EIT and ATS effects are described below. The transmission of a probe laser beam through ^{87}Rb atoms was measured using the experimental setup shown in **Figure 2**. The control and probe laser beams were supplied by

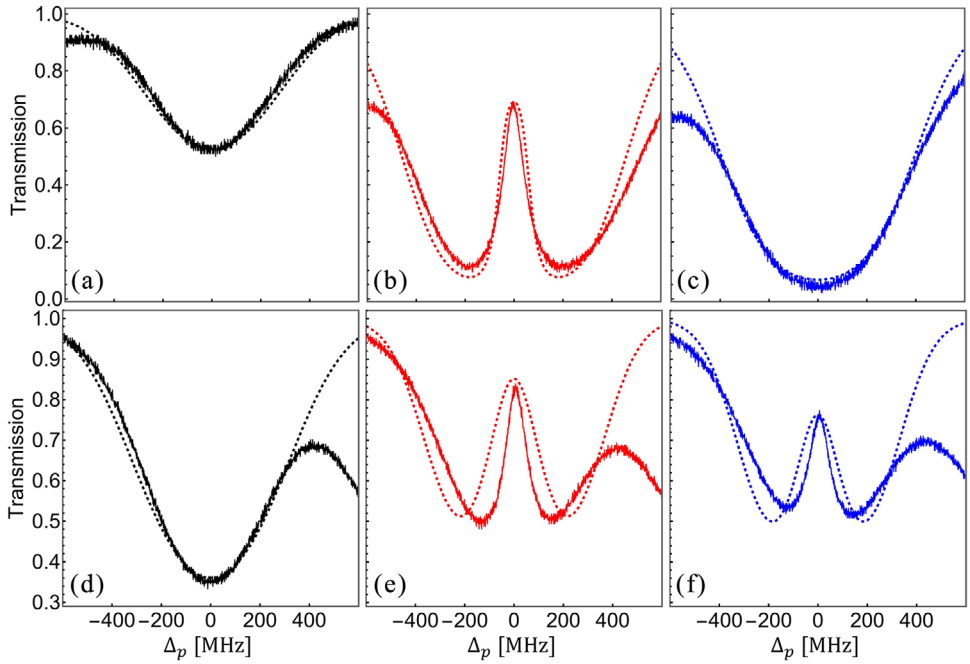

Figure 3. Transmission of the probe field in the EIT (upper panel) and ATS (lower panel) configurations. a,d) Transmission without the control field; b,e) the co-propagation transmission and; c,f) the counter-propagation transmission. Solid curves represent experiment results. Dotted curves are the theoretical fitting.

two independent 795 nm tunable external cavity semiconductor lasers Toptica TA Pro and Toptica DLC Pro). The control field was divided into upper and lower parts. The lower part inputs into a saturation absorption spectroscopy setup and was used to lock the frequency of the control laser to be on resonance with the ^{87}Rb transition of $|5^2S_{1/2}, F = 2\rangle \leftrightarrow |5^2P_{1/2}, F' = 2\rangle$.

The control field in the upper path was injected into the Rb atomic probe vapor cell to modulate the propagation of the probe field. In this experiment, the control field was chosen to propagate through the probe vapor cell in either left-to-right (forward) or right-to-left (backward) direction but the direction of the probe laser beam was fixed. Note that this operation is equivalent to reversing the direction of the probe laser beam[31] and has been widely used in experiments. The control field in the probe vapor cell was vertically polarized. The probe field travelled forward in the probe vapor cell and was horizontally polarized. It drove the transition $|1\rangle \leftrightarrow |3\rangle$ of the D1 line of ^{87}Rb atoms. To reduce noise from the co-propagation control field, the control and probe laser beams were first arranged collinear in the probe atomic vapor cell. Then, the propagation direction of the control laser beam was carefully adjusted to have a tiny angle with the probe one, by tuning the reflective mirrors. In this way, the probe and co-propagation control beams had a large overlap in the probe atomic vapor cell. But their propagation directions had a small angle of about 0.19°. These two laser beams separated by 10 mm on a plane 3 m away. After passing through the probe vapor cell, the co-propagation control beam was separated by a PBS from the probe channel. The counter-propagation control beam was arranged to travel along the opposite direction of the co-propagation control beams. Both the control and probe fields were focused by convex lens with a 10 cm focal length. The detector monitored the probe field intensity when the probe frequency scanned over the relevant atomic transition. The atomic probe vapor cell was 8 cm long and heated to 80°C.

4. Results

We measure the co- and counter-propagation transmissions of the probe field in the EIT and ATS configurations for examining optical nonreciprocity. Throughout our measurement, the probe field power is fixed at $P_p = 3.02\ \mu W$. A stronger probe laser will saturate the atomic medium and then reduce signal level.

First, we characterize the system transmission with the probe beam only. In the absence of the pump field, the atomic vapor is absorptive. The probe scans around the transition $|1\rangle \leftrightarrow |3\rangle$. The measured transmission spectra (black solid curves) of the probe field are shown in **Figure 3**a for the former and in Figure 3d for the latter. It can be seen that the transmission spectrum are Voigt profiles, convolution of a Gaussian distribution with a Lorentzian profile. The spectra are well fitted with the theoretical results (black dotted curves).

The optical nonreciprocity of the EIT effect is evidenced in Figure 3b,c. We compare the probe transmission in the co- and counter-propagation cases by applying an on-resonance control light with power $P_c = 80$ mW and the detuning $\Delta_c = 0$. In the former case, a transmission peak (red solid curve) is clearly observed at the resonance frequency, that is, $\Delta_p = 0$. The peak transmittance is about 68.7%. This is the typical EIT phenomenon. This is well interpreted as the destructive interference of two quantum paths. The EIT peak is well fitted with the model. In the latter case, the probe transmission at the resonance frequency ($\Delta_p = 0$) has a minimum as low as 2.68% (blue solid curve), corresponding to optical nonreciprocity of 14 dB isolation ratio. We fit the experimental data in Figure 3b,c with Equations (3) and (4) (red

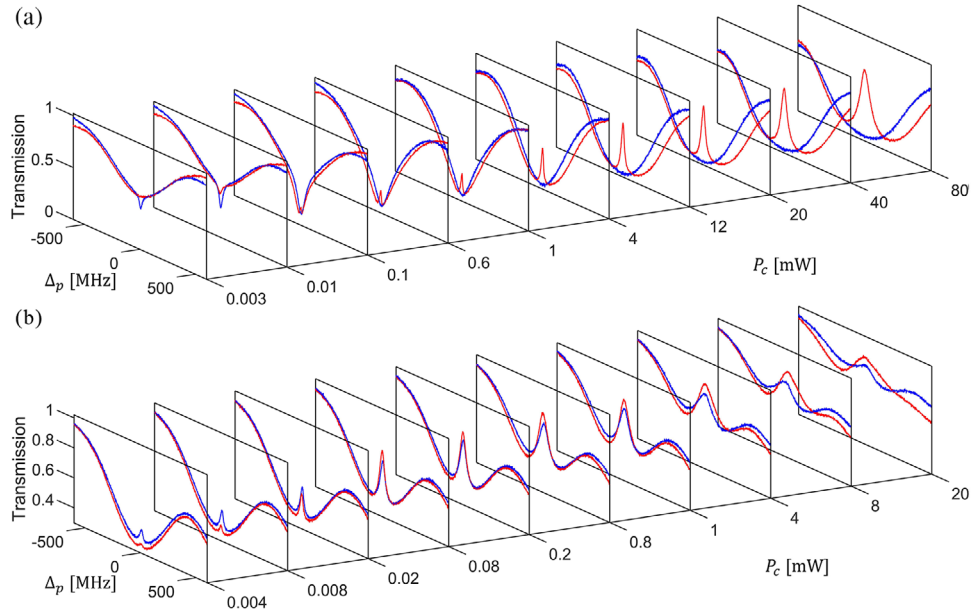

Figure 4. Transmission spectra of the probe field in a) the EIT configuration and b) the ATS configuration. Red curves represent the co-propagation transmission; blue curves are for the counter-propagation transmission.

and blue dashed curves), respectively. The fitting parameters are $N = 6 \times 10^{10}$ cm^{-3}, $\gamma_3 = 2\pi \times 5.7$ MHz, $\Omega_c = 12\gamma_3$, $\Gamma_{21} = 1.2\gamma_3$ and an effective length $L = 8$ cm. Due to thermal pumping of the ground state $|2\rangle$ at finite temperature, the decoherence rate Γ_{21} can be larger than γ_3. Clearly, the theoretical transmission spectra are in good agreement with the experimental results. Note that the minima of the transmissions in Figure 3b,c are smaller than that in Figure 3a due to the repumping of atoms caused by the control field.

In comparison to the EIT effect, the ATS effect is nearly reciprocal, see Figure 3e,f. We apply an on-resonance control light with power $P_c = 800$ μW and the detuning $\Delta_c = 0$. We observe nearly equal transmission at $\Delta_p = 0$, about 83.4% in the co-propagation case and about 75.9% in the counter-propagation case, respectively. We understand the appearance of the transparent window as a result of the ATS. The theoretical results (red dotted curves), calculated according to Equations (9) and (10) with parameters $N = 2.8 \times 10^9$cm^{-3}, $\gamma_3 = 2\pi \times 5.7$ MHz, and $\Omega_c = 30\gamma_3$, are in qualitative agreement with experimental observations. The discrepancy in the peak width mainly results from the derivation of the two-level absorptive model. In this simple model, we neglect the coherence σ_{23} and consider the Zeeman sublevels as a single level. A realistic model including the coherence σ_{23} and multi-Zeeman sublevels can fit the experimental data better.[54,55] However, the model with multi-Zeeman sublevels will be very complicate. To focus on the key point of underlying physics, we use the simple two-level model in the ATS effect to interpret the experimental observation. Note that the control Rabi frequency in the V-type system is much larger than that in the Λ-type system when the same control power is applied. The reasoning is complex. First, the probe and control fields in the former share the common ground state. This makes the coupling very efficient in the V-type system. In contrast, the control field in the latter drives the transition of barely populated states $|2\rangle$ and $|3\rangle$, while the probe field couples to a mostly populated state $|1\rangle$. As a result, the interaction between the control field and atoms is inefficient. Second, the multi-Zeeman levels also cause the difference. However, this effect of multi-Zeeman levels is excluded in our model for simplicity.

Figure 4a,b shows the transmission spectra of the probe field versus the control laser power. We first focus on the co-propagation case of the EIT configuration in Figure 4a. The standard theoretical model of EIT assumes that the ground state related to the probe field is almost completely populated such that $\langle\sigma_{11}\rangle \approx 1$,[1] due to the strong pumping of the control field. When $P_c \leq P_p$, this prerequisite of EIT is invalid. As a result, the transmission spectra are similar to the transmission spectrum of Rb atoms without the control laser. As the control laser power increases but is still comparable with the probe laser, a dip appears in the transmission because the control laser dominantly repumps the state $|1\rangle$ via the incoherent atomic decay and N increases, causing a stronger absorption to the probe field. As the control power increases further to $P_c = 0.1$ mW, about $30P_p$, the atom number populated in the ground state $|1\rangle$ becomes saturated and EIT begins to appear. This indicates EP, $\Omega_c \sim \Omega_c^{EP}$, in the EIT configuration. After that, the transparent peak gradually becomes higher and wider as the control power gets larger, even up to $P_c = 80$ mW. The background absorption vanishes when P_c is large, for example, $P_c = 4$ mW. In the counter-propagation case, the absorption increases and the transmission reduces with the control power. As long as $\Omega_c \gg \Omega_p$, optical nonreciprocity is clearly observed from the weak coupling regime, for example, $P_c = 0.6$ or 1 mW, to the strong coupling regime, even when P_c is very large, reaching 80 mW that $\Omega_c = 12\gamma_3$ by fitting.

The ATS configuration is simple, because a larger control field causes a stronger ATS, see Figure 4b. The transparent peak appears in both the co- and counter-propagation cases when the control power is small, about $P_c = 4$ μW. As the control

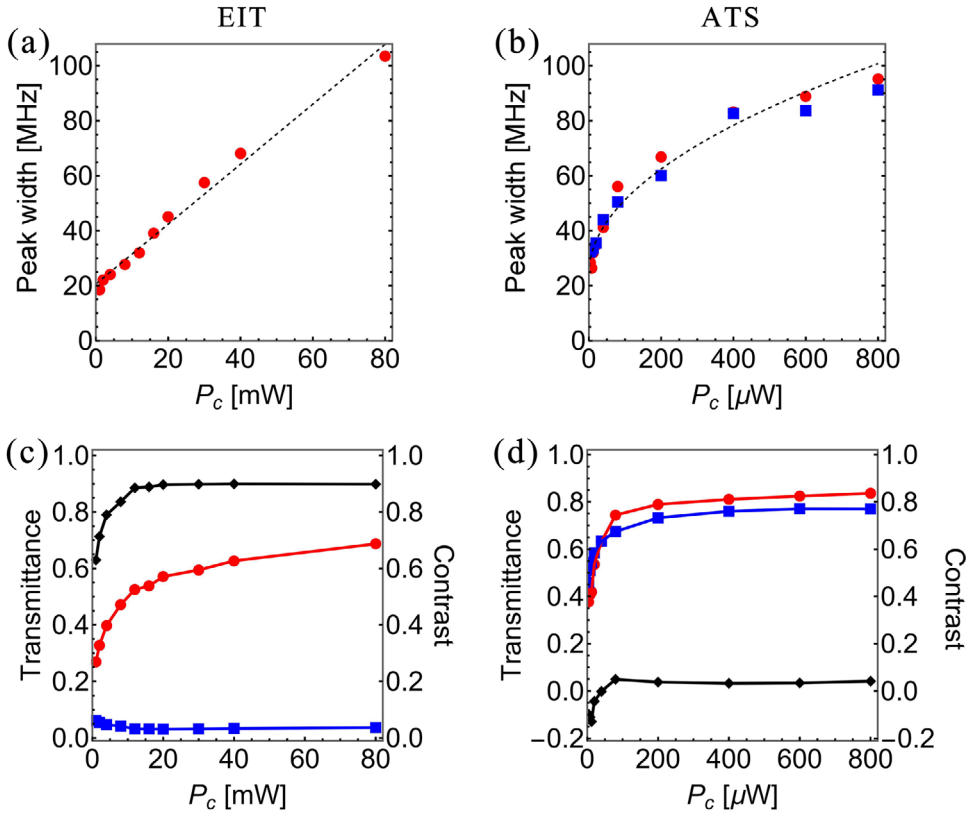

Figure 5. a,b) Peak width of the transmission versus different control laser power. Dashed curves are the fitting of experimental results. In fitting, the unit of the control power is μW. c,d) On-resonance transmission and isolation contrast (black curves and data markers) versus different control laser power, respectively. Red (blue) curves and data markers are for the co-propagation (counter-propagation) transmission. Left panel is for the EIT configuration, and right panel is for the ATS configuration.

power increases, the peaks becomes higher and wider. However, the transmission spectra in two cases are similar for a control laser power up to 2 mW. As a result, optical nonreciprocity is very weak until a strong control field with $P_c > 8$ mW destroys the transmission spectrum. To calibrate the transmission spectrum, we subtract the background noise caused by resulted from the cross-talk of the strong control laser from the detected signal in the EIT experiment and in the ATS experiment when $P_c > 1$ mW.

We measure and fit the widths, δ_{EIT} and δ_{ATS}, of the transmission peaks of the probe field in both configurations when the control laser is strong enough, as shown in **Figure 5**a,b. As the control power varies from 1 to 80 mW in the EIT configuration, the measured peak width of the co-propagation transmission grows linearly with P_c from 18.5 to 103.5 MHz. The experimental data (red dots) is well fitted (dashed line) by a function of δ_{EIT} (MHz) $= 20.62 + 1.09P_c$. In the ATS configuration, the transmission peaks appear in both the co- and counter-propagation cases. The peak width and height are very close. The peak width (red dots and blue squares) in both cases can be fitted (dashed curve) by function δ_{ATS} (MHz) $= 24.17 + 2.7\sqrt{P_c}$. The peak width increases as a function of $\sqrt{P_c}$ from an initial offset about 30 MHz. Note that these fittings are invalid for a weak control field because the incoherent process is dominant. These peak widths include contributions from inhomogeneous broadening and laser phase noise.

Figure 5c,d shows the on-resonance transmission under different control-field power. We observe strong optical nonreciprocity in the EIT configuration. In the AIC-based absorption profile fitting, the transparency in the copropagation case is considered as a gradual transition from the EIT effect to the ATS as the pump laser power increases. In our observation in the copropagation case, the near-resonance probe field ($\Delta \approx 0$) has a high transmission. The peaked transmission increases from 26.9% to 68.7% as we tune the control laser power from 1 to 80 mW. In contrast, the backward transmission is always small. Thus, the corresponding isolation contrast increases to higher than 90%, implying a strong optical nonreciprocity. In this power range, the control-field Rabi frequency is much larger than the criteria value Ω_{EIT}, which indicates a transition from the EIT dominant domain to the ATS overwhelming according to the AIC-based fitting. Even under a very strong control power of $P_c = 80$ mW that the EIT window is much larger than the decoherence rate of atoms γ_3, we still observe a high co-propagation transmission. Obviously, nonreciprocity maintains large in the regime of $\Omega_c \gg \Omega_{EIT}$.

Contrary to the EIT effect, the ATS effect causes little optical nonreciprocity to the probe propagation although atoms are still subject to the microscopic Doppler effect. We observe the similar transmission spectra of the probe field in the V-type atomic ensemble in the co- and counter-propagation cases, see Figure 4c,d. In both cases, the ATS induces transparent windows. The transmission difference in two cases slightly

increases with the control laser power but remains small. The difference is about 7.5% when P_c increases up to 800 μW, maintaining a very weak optical nonreciprocity. The essentially different capability of EIT and ATS in breaking the time-reversal symmetry, indicates that the appearance of the transparency peak in a Λ-type system in the strong control regime due to EIT, an effect different from ATS. The transition of transparent profile in EIT is because the system crosses EP as discussed in our theoretical analysis. This is the main finding of this work.

The microscopic Doppler effect can be used to achieve strong all-optical isolation in cavity-EIT system[31] or a Ladder-type EIT system.[35] Here our Λ-type EIT system can also operate as an all-optical isolator because the opposite transmissions can be very different. The available isolation contrast is limited by several factors in experiment. To achieve a high isolation contrast, one needs a large forward transmission of the probe field in the co-propagation and a small backward transmission in the counter-propagation. The forward transmission becomes quickly saturated as the control laser field increases. Thus, in practice, a vanishing small backward transmission is preferable. However, the background noise sets the reliable minimal value of the backward transmission. In this sense, the available isolation contrast is mainly limited by the background noise in the counter-propagation case. Due to the limited measurement accuracy and noise in our experiment, the backward transmission is bounded to 1–3%. As a result, the maximal isolation contrast we can achieve is 92.7%.

5. Conclusion and Discussion

By observing the directional transmission of a probe field in the EIT and ATS configurations from the weak control regime to the strong control regime, we have experimentally proved that the EIT and the ATS of atoms are essentially different in breaking the TRS. Thermal motion of atoms in the Λ-type system exhibiting EIT can induce the SML and cause strong optical nonreciprocity to the probe field. In sharp contrast, the ATS effect is primarily reciprocal. Our work opens a new door to exploit the nonreciprocity as a powerful testbed for distinguishing subtle physic effects with similar phenomena at the fundamental level.

Note that our method is not suited for distinguishing the EIT and effects in a solid-state system or cold atoms, owing to the lack of the Doppler effect. However, it exploits the thermal-motion induced SML to show the fact that the EIT and ATS are fundamentally different effects.

Acknowledgements

H.W. and Y.R. contributed equally to this work. This work was supported by the National Key R&D Program of China (Grants No. 2019YFA0308700, No. 2019YFA0308704, and No. 2017YFA0303703), the National Natural Science Foundation of China (Grant No. 11874212 and No.11890704), the Program for Innovative Talents and Teams in Jiangsu (Grant No. JSSCTD202138), and the Excellent Research Program of Nanjing University (Grant No. ZYJH002).

Conflict of Interest

The authors declare no conflict of interest.

Data Availability Statement

The data that support the findings of this study are available from the corresponding author upon reasonable request.

Keywords

Autler–Townes splitting, electromagnetically induced transparency, nonreciprocity

Received: December 11, 2021
Revised: April 30, 2022
Published online: July 3, 2022

[1] M. Fleischhauer, A. Imamoglu, J. P. Marangos, *Rev. Mod. Phys.* **2005**, *77*, 633.
[2] S. H. Autler, C. H. Townes, *Phys. Rev.* **1955**, *100*, 703.
[3] B. W. Shore, *The Theory of Coherent Atomic Excitation (Vol. I): Simple Atoms and Fields*, John Wiley & Sons, New York **1990**.
[4] S. E. Harris, *Phys. Today* **1997**, *50*, 36.
[5] Y.-q. Li, M. Xiao, *Phys. Rev. A* **1995**, *51*, 4959.
[6] S. Weis, R. Rivière, S. Deléglise, E. Gavartin, O. Arcizet, A. Schliesser, T. J. Kippenberg, *Science* **2010**, *330*, 1520.
[7] H. Jing, Ş. K. Özdemir, Z. Geng, J. Zhang, X.-Y. Lü, B. Peng, L. Yang, F. Nori, *Sci. Rep.* **2015**, *5*, 9663.
[8] G. Andersson, M. K. Ekström, P. Delsing, *Phys. Rev. Lett.* **2020**, *124*, 240402.
[9] C. Wang, X. Jiang, G. Zhao, M. Zhang, C. W. Hsu, B. Peng, A. D. Stone, L. Jiang, L. Yang, *Nat. Phys.* **2020**, *16*, 334.
[10] K. Totsuka, N. Kobayashi, M. Tomita, *Phys. Rev. Lett.* **2007**, *98*, 213904.
[11] C. Wang, X. Jiang, W. R. Sweeney, C. W. Hsu, G. Zhao, B. Peng, M. Zhang, L. Jiang, A. D. Stone, L. Yang, *Proc. Natl. Acad. Sci. U. S. A.* **2021**, *118*, e2012982118.
[12] S. Novikov, T. Sweeney, J. E. Robinson, S. P. Premaratne, B. Suri, F. C. Wellstood, B. S. Palmer, *Nat. Phys.* **2016**, *12*, 75.
[13] S. Zhang, D. A. Genov, Y. Wang, M. Liu, X. Zhang, *Phys. Rev. Lett.* **2008**, *101*, 047401.
[14] M. Mücke, E. Figueroa, J. Bochmann, C. Hahn, K. Murr, S. Ritter, C. J. Villas-Boas, G. Rempe, *Nature (London)* **2010**, *465*, 755.
[15] H. Wu, J. Gea-Banacloche, M. Xiao, *Phys. Rev. Lett.* **2008**, *100*, 173602.
[16] Y. Zhu, *Opt. Lett.* **2010**, *35*, 303.
[17] K. Xia, J. Evers, *Phys. Rev. Lett.* **2009**, *103*, 227203.
[18] A. V. Gorshkov, A. André, M. D. Lukin, A. S. Sørensen, *Phys. Rev. A* **2007**, *76*, 033804.
[19] Y.-H. Chen, M.-J. Lee, W. Hung, Y.-C. Chen, Y.-F. Chen, I. A. Yu, *Phys. Rev. Lett.* **2012**, *108*, 173603.
[20] M. Fleischhauer, A. S. Manka, *Phys. Rev. A* **1996**, *54*, 794.
[21] M. D. Eisaman, A. André, F. Massou, M. Fleischhauer, A. S. Zibrov, M. D. Lukin, *Nature (London)* **2005**, *438*, 837.
[22] H. Schmidt, A. Imamoglu, *Opt. Lett.* **1996**, *21*, 1936.
[23] H. Wang, D. J. Goorskey, M. Xiao, *J. Mod. Opt.* **2002**, *49*, 335.
[24] S. Rebić, J. Twamley, G. J. Milburn, *Phys. Rev. Lett.* **2009**, *103*, 150503.
[25] M. D. Lukin, A. Imamoğlu, *Phys. Rev. Lett.* **2000**, *84*, 1419.
[26] Z.-Y. Liu, Y.-H. Chen, Y.-C. Chen, H.-Y. Lo, P.-J. Tsai, I. A. Yu, Y.-C. Chen, Y.-F. Chen, *Phys. Rev. Lett.* **2016**, *117*, 203601.
[27] S. Li, X. Yang, X. Cao, C. Zhang, C. Xie, H. Wang, *Phys. Rev. Lett.* **2008**, *101*, 073602.
[28] H. Kang, L. Wen, Y. Zhu, *Phys. Rev. A* **2003**, *68*, 063806.
[29] J. Sheng, X. Yang, H. Wu, M. Xiao, *Phys. Rev. A* **2011**, *84*, 053820.
[30] X. Lu, W. Cao, W. Yi, H. Shen, Y. Xiao, *Phys. Rev. Lett.* **2021**, *126*, 223603.

[31] S. Zhang, Y. Hu, G. Lin, Y. Niu, K. Xia, J. Gong, S. Gong, *Nat. Photonics* **2018**, *12*, 744.
[32] E.-Z. Li, D.-S. Ding, Y.-C. Yu, M.-X. Dong, L. Zeng, W.-H. Zhang, Y.-H. Ye, H.-Z. Wu, Z.-H. Zhu, W. Gao, G.-C. Guo, B.-S. Shi, *Phys. Rev. Res.* **2020**, *2*, 033517.
[33] C. Liang, B. Liu, A.-N. Xu, X. Wen, C. Lu, K. Xia, M. K. Tey, Y.-C. Liu, L. You, *Phys. Rev. Lett.* **2020**, *125*, 123901.
[34] K. Xia, F. Nori, M. Xiao, *Phys. Rev. Lett.* **2018**, *121*, 203602.
[35] M.-X. Dong, K.-Y. Xia, W.-H. Zhang, Y.-C. Yu, Y.-H. Ye, E.-Z. Li, L. Zeng, D.-S. Ding, B.-S. Shi, G.-C. Guo, F. Nori, *Sci. Adv.* **2021**, *7*, eabe8924.
[36] P. Tamarat, T. Gaebel, J. R. Rabeau, M. Khan, A. D. Greentree, H. Wilson, L. C. L. Hollenberg, S. Prawer, P. Hemmer, F. Jelezko, J. Wrachtrup, *Phys. Rev. Lett.* **2006**, *97*, 083002.
[37] C.-K. Yong, J. Horng, Y. Shen, H. Cai, A. Wang, C.-S. Yang, C.-K. Lin, S. Zhao, K. Watanabe, T. Taniguchi, S. Tongay, F. Wang, *Nat. Phys.* **2018**, *14*, 1092.
[38] C.-K. Yong, M. I. B. Utama, C. S. Ong, T. Cao, E. C. Regan, J. Horng, Y. Shen, H. Cai, K. Watanabe, T. Taniguchi, S. Tongay, H. Deng, A. Zettl, S. G. Louie, F. Wang, *Nat. Mater.* **2019**, *18*, 1065.
[39] P. D. Cunningham, A. T. Hanbicki, T. L. Reinecke, K. M. McCreary, B. T. Jonker, *Nat. Commun.* **2019**, *10*, 5539.
[40] K. Xia, J. Twamley, *Phys. Rev. X* **2013**, *3*, 031013.
[41] E. Saglamyurek, T. Hrushevskyi, A. Rastogi, K. Heshami, L. J. LeBlanc, *Nat. Photon.* **2018**, *12*, 774.
[42] L. Tang, J. Tang, W. Zhang, G. Lu, H. Zhang, Y. Zhang, K. Xia, M. Xiao, *Phys. Rev. A* **2019**, *99*, 043833.
[43] A. Lazoudis, T. Kirova, E. H. Ahmed, P. Qi, J. Huennekens, A. M. Lyyra, *Phys. Rev. A* **2011**, *83*, 063419.
[44] C. Wei, N. B. Manson, J. P. D. Martin, *Phys. Rev. A* **1995**, *51*, 1438.
[45] S. Li, X. Yang, X. Cao, C. Xie, H. Wang, *J. Phys. B: At. Mol. Opt. Phys.* **2007**, *40*, 3211.
[46] C. Zhu, C. Tan, G. Huang, *Phys. Rev. A* **2013**, *87*, 043813.
[47] L. Hao, Y. Jiao, Y. Xue, X. Han, S. Bai, J. Zhao, G. Raithel, *New J. Phys.* **2018**, *20*, 073024.
[48] S. K. Nath, V. Naik, A. Chakrabarti, A. Ray, *J. Opt. Soc. Am. B* **2019**, *36*, 2610.
[49] P. M. Anisimov, J. P. Dowling, B. C. Sanders, *Phys. Rev. Lett.* **2011**, *107*, 163604.
[50] L. Giner, L. Veissier, B. Sparkes, A. S. Sheremet, A. Nicolas, O. S. Mishina, M. Scherman, S. Burks, I. Shomroni, D. V. Kupriyanov, P. K. Lam, E. Giacobino, J. Laurat, *Phys. Rev. A* **2013**, *87*, 013823.
[51] B. Peng, S. K. Özdemir, W. Chen, F. Nori, L. Yang, *Nat. Commun.* **2014**, *5*, 5082.
[52] Z. Ji, Y. Jiao, Y. Xue, L. Hao, J. Zhao, S. Jia, *Opt. Express* **2021**, *29*, 11406.
[53] J. Liu, H. Yang, C. Wang, K. Xu, J. Xiao, *Sci. Rep.* **2016**, *6*, 19040.
[54] B. Wang, Y. Han, J. Xiao, X. Yang, C. Zhang, H. Wang, M. Xiao, K. Peng, *Phys. Rev. A* **2007**, *75*, 051801.
[55] H. Y. Ling, Y.-Q. Li, M. Xiao, *Phys. Rev. A* **1996**, *53*, 1014.